Influence of spray-glow plug configuration on cold start combustion for high-speed direct injection diesel engines

J.V. Pastor*, V. Bermúdez, J.M. García-Oliver, J.G. Ramírez-Hernández

CMT Motores Térmicos - Universidad Politécnica de Valencia
Camino Vera s/n - 46022 Valencia, Spain.
Telephone: +34 963877650, Fax: +34 963877659

Abstract

Glow plugs are currently the most employed solution to promote ignition in light duty diesel engines during low temperature cold start. Improved knowledge about the mechanisms that control ignition and flame development under such conditions is necessary for design purposes, especially with current trends to reduce engine compression ratio. This paper aims to analyze the influence of the glow plug configuration (disposition and temperature) on cold start combustion. Experimental tests carried out in an optical engine with high speed visualization have confirmed that the spray-glow plug configuration influences the whole combustion process through pilot ignition. Ignition of pilot injection is controlled by glow plug temperature and by the fuel and air motion after the end of injection. Nevertheless, the glow plug temperature effect starts to be negligible over certain value since chemical ignition delay cannot be further reduced. For this reason, the path to follow is to increase the amount of fuel that reaches the glow plug, which is directly

*Corresponding author
Email address: jpastor@mot.upv.es (J.V. Pastor)

related with the flow motion in the cylinder after injection.

Keywords: Diesel, Combustion, Cold start, Glow plug, Ignition

---

[Table 1 about here.]

1. Introduction

In spite of all the improvements made in diesel technology to date, engine starting is still a problem for current light duty engines at low ambient temperature and it is a limiting factor for future design trends. Depending on ambient temperature, the starting process of a diesel passenger car engine may result in long cranking periods with a large amount of pollutant emissions [1, 2, 3, 4] or in the complete incapability of starting the engine. These problems are caused by the poor ignition conditions reached within the combustion chamber of low-compression ratio engines at low ambient temperatures. Specifically, these poor ignition conditions are the consequence of, on the one hand, the relatively low peak compression temperature which causes poor vaporization and increases chemical delays. On the other hand, they are consequence of the low peak compression pressure due to the high blow-by level as a result of low engine block temperature, low engine speed and low intake pressure. As a reference, Broatch *et al* [5] reports that a light duty diesel engine (CR 18:1) can start without aid at temperatures as low as $-11°C$. At lower temperatures, ignition aids become necessary. In future applications, in which the compression ratio is reduced [6, 7, 8] to comply with the near future emissions standards [9, 10], starting aids will be necessary at ambient temperatures below $10°C$ (tested in a 14:1 CR engine [5]). For all these reasons, the appropriate use and optimization of the starting aids

are necessary in order to overcome present and future limitations of diesel passenger car engines.

Two pre-heating procedures have been commonly employed in diesel engines: heating all the gas entering in the cylinder or generating a hot spot in the combustion chamber. In the first solution, a heater in the intake system is used to warming up all the air aspirated by the cylinder. This is the solution employed in medium and large diesel engines and it has only being evaluated for cold starting of small modern diesel engines [11]. In the other solution, which is imported from IDI diesel engines, a glow plug is assembled in the cylinder head, so that its tip protrudes into the combustion chamber. Due to the low amount of heat transferred to the surroundings [12], the glow plug only works as a hot spot within the cylinder. This solution is the most extensively used aid in small and medium sized engines [13, 14]. It presents the disadvantage of being an intrusive element protruding in the combustion chamber, which can have an adverse influence on combustion in normal engine operation.

In spite of being largely employed in small modern diesel engines, few reliable information is available on the role of glow plug during start and how to improve its disposition within the combustion chamber. This device, according to manufacturers [13, 14], is made to reach a temperature of 1250 K in a few seconds and it should be located in such way that the heater rod surface of the glow plug contacts the rim zone of the spray. Besides that, not much more information has been found about the real glow plug temperature or the methods employed to measure this temperature. Regarding the disposition of the glow plug within the chamber, two studies have allowed to shed some

light on how to optimize it. On the one hand, Pacaud *et all* [6] proposes different ways to improve cold start operation for a low compression ratio engine (13.7:1) at $-20°C$, and two of these ways are directly related with the glow plug-spray configuration. First, Pacaud *et all* [6] variates the nozzle tip protrusion by changing the spacer rings located below the injector, which was vertically mounted. They found that engine start delay decreases as the nozzle tip protrusion does, which coincides with a decrement of the distance between the glow plug tip and the injector spray axes. In second place, they changed the orientation angle between one of the sprays and the glow plug by rotating the injector. They found very different results for two configurations with the same spray to glow plug distance, being the best of the two the one at which the spray was oriented in the up-swirl direction. They attribute this result to the swirl motion within the chamber. These results only allow to shed some light on the parameters that affect combustion and to propose hypothesis on what could be going on within the chamber, they do not show how glow plug disposition influences the ignition mechanisms. On the other hand, Walter *et all* [15] give a step forward and add combustion visualization to its study. The main contribution of this work is that they show that glow plug configuration and disposition parameters have an effect only on pilot injection and they also add the glow plug temperature as another possible influence parameter. But, a larger statistical sample would be necessary in order to account with cycle to cycle dispersion, which is typical under such conditions [16]

In a previous work presented by the authors [17], a description of the mechanisms that lead to pilot ignition was presented as a basis to understand

further parametric variations. In that paper, the importance of the glow plug surface as the only possible ignition spot is confirmed. And, it is shown, with a large statistical sample, that ignition occurs only after the end of injection. For this reason, transport processes that carry the fuel to the glow plug after injection were found to have remarked importance. In the same way, it was found that these transport processes can be controlled indirectly by means of rail pressure and injection pulse duration. The aim of the present work is to find out the role that glow plug has on the whole sequence of events that lead to ignition and its importance compared with the transport processes controlled by the injection event. Results obtained will also give guidelines for engine design and calibration of real engines and glow plugs. This document has been structured as follows. After this introduction, a brief description of the experimental and theoretical tools employed is presented. Then, results are divided in two separated sections. First, it is shown the influence of the disposition of the glow plug with respect to one of the sprays. Secondly, the influence of the glow plug temperature is presented. Finally, the main outcomes are summarized.

2. Tools and methodology

2.1. Combustion visualization

In order to perform combustion visualization studies, a methodology has been developed and an experimental facility has been adapted to reproduce, at room temperature, in-cylinder thermodynamic conditions representative of those of a real passenger car engine during start at low ambient temperature [5]. A complete description of this experimental facility and methodol-

ogy has been previously reported in [16]. This sub-section only shows a brief summary of the main contents.

2.1.1. Experimental facility

A 4-valve and 0.55 l displacement single cylinder optical engine is used in the present study (sketched in Figure 1). It is equipped with an elongated piston with a cylindrical bowl, with dimensions of 45 x 16 mm ($diameter$ x $depth$), which allows optical access to the combustion chamber through a sapphire window placed in its bottom. Below the piston bowl, an elliptical UV mirror is centered on the cylinder axis. In front of the mirror, the high speed camera is positioned to record radiation that comes from the combustion chamber.

[Figure 1 about here.]

The facility has been modified to reproduce the first injection cycle of the starting sequence of a passenger car engine at $-20°C$. Specifically, thermodynamic conditions within the combustion chamber (temperature and pressure [5]) and low engine speed can be reproduced systematically [16]. In order to reach the low peak in-cylinder temperature, the compression ratio has been reduced (from 16:1 to 8:1) and intake temperature has been controlled at $30°C$. Compression ratio has been reduced by placing an aluminum piece (shown in Figure 1), with 42 mm height and internal diameter slightly larger than the engine bore, between the cylinder head and the engine block. Peak in-cylinder pressure has been set controlling the intake pressure. And, low engine speed (250 rpm) has been achieved by modifying the electronics of the electrical motor.

A common rail injection system with piezo-injectors is operated externally to ensure stable behavior avoiding uncertainties associated to corrections made by the ECU. The injector used is equipped with a microsac nozzle with six holes (with a nominal diameter of 0.121 mm). It is centered in the cylinder and vertically mounted as shown in Figure 1. In that way, spray orientation with respect to the glow plug can be modified by rotating the injector around its axis. Injection is performed at a reduced frequency (one injection every 40 cycles) to avoid engine temperature increase, speed instability in case of ignition and to reduce window fouling.

2.1.2. In-cylinder pressure analysis

The tool employed to perform combustion analysis is the one-zone model CALMEC, which is better described in [18]. This diagnosis tool uses the measured in-cylinder pressure as main input. Then, the first law of thermodynamic is applied between IVC and EVO considering the chamber as an open system because of blow-by and fuel injection. The ideal gas equation of state is used to calculate the mean gas temperature in the chamber. Along with these two basic equations, several sub-models are used to calculate instantaneous volume, heat transfer [19] and mass transfer, among others. The model main result is the ROHR. But the temporal evolution of other parameters like the HRL (defined as the integral of ROHR and normalized with respect to its maximum) or the mean gas temperature can be calculated. Temporal resolution for these variables depends on the crank angle encoder configuration (0.5 CAD). Global information on each cycle can be obtained, such as IMEP, SOC and CE. SOC is defined as the crank angle position where the beginning of the steep rise in ROHR due to combustion is detected. CE

is defined as the ratio between the total energy released in one cycle and the total energy available in the fuel injected. It is calculated by equation 1:

$$CE = \frac{100}{m_f \cdot LHV} \cdot \int_{IVC}^{EVO} ROHR(\alpha)\, d\alpha \tag{1}$$

where the energy released in one cycle is the integral of the ROHR calculated between IVC and EVO, m_f is the mass of fuel injected and LHV is the fuel lower heating value.

2.1.3. Image acquisition and post-processing

Optical techniques have been applied along the years in spray and combustion characterization studies as recently reviewed by Soid and Zainal in [20]. Under non-conventional engine conditions, imaging tools become specially useful to explain different phenomena that can not be observed with classical tools [21]. Direct visualization has been used in this study for characterization of the whole combustion sequence, with special emphasis on pilot ignition and development, which cannot be properly studied with only the pressure trace.

Images were recorded using a Photron Ultima APX high speed camera. It is equipped with a 10-bit CMOS sensor and all images in the study have been recorded at an acquisition frequency of 6000 fps with a 512 x 512-pixels image size. The camera has been coupled with a $135 - 400$ mm focal length Helmut APO objective with a number 1 close up lens.

In order to simplify combustion analysis, time resolved parameters are obtained for every image sequence by means of post-processing. First, segmentation is performed for every single image by calculating a threshold value which is equal to the minimum digital level in the image (found in

a zone without any combustion luminosity) plus 15% of the difference between the maximum and the minimum. This percentage has been chosen as a compromise to eliminate light reflected on the liquid spray and the chamber walls without losing much information from the combustion event. After segmentation, the digital levels of all pixels containing the combustion radiation (with digital levels above the threshold) are accumulated in a single parameter named I_{cumul}. Additionally, as shown in Figure 2, IL is defined as the integral of the I_{cumul} plot and LD as the time between SoI and the first luminosity detection.

[Figure 2 about here.]

2.2. Modeling tools

2.2.1. Chemical kinetics

Calculations have been performed by means of CHEMKIN software [22]. An n-Heptane detailed kinetic mechanism [23], considered as suitable diesel fuel surrogate in terms of ignition characteristics, has been solved for constant pressure homogeneous reactor conditions. Simulations have spanned a range between 600 and 1200 K in terms of initial temperatures, and 0.2 to 2 in terms of fuel equivalence ratio. Pressure has been set to 27 *bar* for all cases (in-cylinder pressure at SoI). Ignition delay has been defined as the time period from start of calculations until an increase of 400 K, over the initial temperature, is detected.

2.2.2. CFD calculations

Simulations have been performed by means of StarCD [24] to understand the physical processes related to fuel evaporation and mixture formation

from SoI until flame appearance. For this reason, no combustion model has been used. The computational grid comprised the combustion chamber and crevice volumes as well as the glow-plug. Typical grid size is around 1 mm, and it is further refined around the glow plug region. A standard lagrangian approach (DDM[25]) is used for fuel spray modeling. Huh-Gosman [26] and Reitz-Diwakar [27] models are applied for primary and secondary break-up, respectively. Spray outlet boundary conditions are obtained from injection mass flow rate and momentum flux measurements. Fuel physical properties are given by the so-called DF1 [28] diesel fuel surrogate. Turbulent flow is modeled with the RNG $k-\epsilon$ model and standard wall functions. Both, initial conditions at IVC and wall temperatures, have been estimated by means of CALMEC [18] from experimental data. A wheel-flow velocity profile with swirl number 2.2 is used for air-flow initialization, and a constant temperature boundary condition (1250 K) is applied on the glow plug surface.

2.3. Conditions of the study

During combustion visualization tests, basic engine conditions were kept unchanged in the cycles preceding the one with injection. The engine was motored at a stable speed of 250 rpm [16]. Intake air, oil and water temperature were kept fixed at 30°C. Intake pressure was set to reach target peak compression pressure (27 bar). With these engine settings in-cylinder temperature and density have been estimated to be 345°C (618 K) and 16 kg/m^3, which are representative of low temperature cold start cranking process [5].

On this basis, two different injection strategies have been tested. In one set of tests, a full (pilot + main) injection strategy, which is commonly used under cold start conditions [29], and consists on a small pulse of 6 mg

injected at 0 CAD and a larger one of 44 mg injected at 5 CAD. When using this strategy, engine transducers signals have been acquired for 30 injection cycles, images were taken only for the first ten injection cycles due to window fouling. In a second set of tests, the single pilot injection have been isolated in order to study only the ignition phenomena. With this purpose, the camera exposure time has been enlarged to record the low intensity pilot flame using the whole dynamic range. When using this strategy, 20 injection cycles have been recorded for both, engine signals and images.

Two levels of rail pressure have been tested, namely 200 and 370 bar. The former is the lowest possible value for stable behavior at short injection pulses (checked in the mass flow rate measurements). And the latter is a value close to the limit above which ignition can not been achieved in this engine configuration, as shown in a previous work [17].

A standard glow plug [13] have been used for this study. In its normal configuration, the tip protrudes 3 mm into the combustion chamber from the cylinder head plane, it is located at 11.5 mm from the cylinder axis, it is oriented at 10° with respect to the glow plug in the direction of the swirl and it is operated at a constant nominal tension of 11 V. From this standard configuration, parametric variations have been performed as summarized on Table 2 and illustrated in Figure 3. First, the orientation angle have been change by rotating the injector and it has been measured by means of visualization. It is shown in the figure how the orientation angle grows with positive values in the swirl direction and the position at which the spray impacts directly against the glow plug corresponds to 0°. Secondly, glow plug and nozzle tip protrusion have been variated by changing their respective

spacer rings. The distance d between the glow plug surface and the spray axis has been estimated and it is shown in Table 3. Finally, the glow plug temperature has been changed by modifying its supply tension, which has been directly measured on the glow plug terminals.

[Table 2 about here.]

[Figure 3 about here.]

[Table 3 about here.]

3. Influence of the glow plug position relative to spray

3.1. Full injection strategy

As shown in [17], the full injection strategy comprises two different but related problems. First, pilot injection ignition, which is delimited to the interaction between the glow plug and one of the sprays. If pilot injection ignites, it forms a high temperature and localized near-to-the-glow-plug pilot flame that is responsible of promoting main combustion start. The second problem is the main combustion development within the combustion chamber. The relationship between these two problems is shown in Figure 4. On the left side of the figure, the IMEP is plotted versus SOC for the 30 repetitions of a given test. And on the right side, ROHR is plotted versus the crank angle position for two selected cycles of the left side plot. This figure shows the influence that SOC has on IMEP. In cycles at which combustion starts during the injection process (blue cycle on the right plot), combustion rates are considerably higher than for cycles with delayed ignition (red cycle on the right plot). For early burning cycles, combustion duration is also

shorter and better controlled since its progress is promoted by the injection event. On real engine cold start, high IMEP values are desirable because it is necessary to overcome mechanical losses and speed up the engine. As well, the repetitive appearance of these kind of cycles will lead to engine start in a shorter period of time. It must also be taken into account that high IMEP values mean a more efficient process ($CE \propto IMEP$, $R^2 = 0.9708$) which would mean, at the same time, a shorter amount of UHC emissions.

[Figure 4 about here.]

Figures 5 and 6 evidence that the relationship between ignition and combustion progression, explained in the last paragraph, exists under different configurations. Each figure shows the IMEP and SOC as a function of the spray-glow plug orientation angle in Box-Whisker plots. Results at both levels of rail pressure are shown with the purpose of showing two very different conditions and in order to validate hypotheses with a larger experimental sample. In these figures, the relationship explained previously and shown in Figure 4 is confirmed: for cases at which combustion starts earlier the IMEP is notably higher. In addition, it is shown that the distance between the spray and the glow plug has an effect on SOC and IMEP, since the higher IMEP values are reached for configurations at which the spray is oriented near the glow plug. Furthermore, it is observed, for the high rail pressure case in Figure 6, that IMEP values are notably higher if the spray is oriented in the up-swirl direction. This is a similar effect to the one reported Pacaud *et al.* [6] which was attributed to swirl.

[Figure 5 about here.]

[Figure 6 about here.]

Further evidence on the influence on combustion of the distance between the glow plug and the closest spray is shown in Figure 7, where SOC and IMEP are plotted as a function of spray-glow plug distance for the low rail pressure level case. The tests shown in the figure correspond to the NTP and GPP variations at a constant orientation angle of 10°. Figure 7 shows that the spray-glow plug distance does have an influence on SOC and hence on IMEP. This influence is marked above certain distance value. If the distance is short (from 1.78 to 3.51 mm), high combustion probability (above 90%) and high IMEP values are observed in general, with slightly higher values when the glow plug is at 1.78 and 2.22 mm. For the longer distance case (at 4.15 mm), the situation abruptly changes: combustion probability decreases to 30% and IMEP values become considerably lower. These results confirm that the spray-glow plug distance is an important factor with influence on combustion. But, it is also clear that this influence is not due to the contact of the spray with the glow plug. For a distance value of 3.51 mm, for which ignition conditions are good, the half spray angle would have to be greater than 20° to ensure contact, which is not expected for the conditions considered.

[Figure 7 about here.]

The role of pilot injection within the whole combustion sequence is to ensure that combustion takes place and, if it does, that it starts early during the injection event. Figure 8 shows that pilot injection actually is a controlling parameter in order to get high IMEP combustion cycles. In this figure, the appearance probability of early burning cycles ($IMEP > 0$

and $SOC < EOI$) is plotted as a function of the probability of pilot flame appearance($I_{cummul} > 0$) before 5 CAD. These tests were performed independently but keeping pilot injection settings the same; combustion probability corresponds to full injection strategy tests and pilot probability is for single pilot tests. This figure shows very good correlation between both probability values and it leads to the conclusion that combustion start of early burning cycles is controlled by pilot flame. Summarizing, the orientation and the distance of the spray closest to the glow plug does have an influence on main combustion through SOC, which at the same time is controlled by pilot injection.

[Figure 8 about here.]

3.2. Pilot injection

Due to its proved relevance the main combustion promoter, pilot injection is isolated and shown in this sub-section in order to shed some light on its ignition mechanisms. Figures 9 and 10 show LD and IL as a function of the spray-glow plug orientation angle for two very different ignition stability situations, low and high rail pressure. Each test consists on 20 recorded repetitions and the plots are built with the cycles that show luminosity. Important effects are observed in these figures. First, the effect of rail pressure (previously explained in [17]) can be clearly seen: for a constant total injected mass, a higher rail pressure level implies higher fuel velocities and hence a larger amount of fuel misses the glow plug area traveling toward the piston wall. In other words, a rail pressure increase provokes a reduction in the fuel to air ratio near to the glow plug, which reduces ignition probability

and IL, and delays ignition. Secondly, it is shown how the first luminosity is detected in all cases after EoI, confirming that ignition occurs not due to the contact between the spray and the glow plug but due to the convection of fuel after EoI. In this sense, it is also observed that the best configuration is the one at which the spray is oriented at 10° in up-swirl direction. Whatsmore, shorter LD values and higher IL intensities are obtained if the spray is oriented in up-swirl direction compared to the down-swirl direction, for the same absolute angle value. These results show, for a large experimental sample which includes two very different ignition stability situations, that the fuel transport processes that occur after EoI have a strong influence on the mechanisms that lead to ignition.

[Figure 9 about here.]

[Figure 10 about here.]

In order to gain more insight into the fuel transport processes that occur before ignition, Figure 11 combines experimental data, pilot luminosity and mass flow rate, with detailed numerical information about mixing and fuel motion. It is shown for a single pilot injection at low rail pressure. The experimental information on the figure consists on the mass flow rate per orifice, which is a reference to the injection event, and the I_{cummul} trace of five different repetitions, which serve as a reference of the start of luminosity. On the other hand, the numerical information consists on fuel and air speeds (maximum and minimum for each of them) in the spray axis, which can give an idea of the governing motion as a function of time, and fuel to air ratio on the glow plug close vicinity, which together with the glow plug temperature

governs ignition. The ignition sequence starts with the injection event, liquid fuel enters into the combustion chamber at relatively high speed transferring moment to the surrounding air. Due to the low amount of fuel injected, stabilization is never reached and fuel speed increases until the needle starts closing. During injection, the relatively high fuel speed provokes that fuel droplets travel from the nozzle hole directly toward the piston bowl walls and induces the generation of air vortexes. Within this period, fuel residence time on the glow plug vicinity is short, so that low fuel to air ratio values in this area are achieved. Then, the nozzle starts closing, fuel droplets decelerate and the speed difference between fuel and air becomes less and less important with time. This deceleration process of the spray coincides with an fuel to air ratio increase, which is the result of the fuel being dragged to the glow plug by the air vortexes generated earlier during injection and illustrated on Figure 12. After EoI, fuel is driven by the air vortexes and the glow plug vicinity is further enriched by on coming fuel. During this period, only small differences between fuel and air speed are observed, for which it is not surprising that swirl motion has an effect on pilot ignition. After that, fuel to air ratio reaches a maximum value and starts decreasing. In some moment after EoI and depending on complex chemistry mechanisms ignition will occur on the glow plug surface. This whole sequence remark the importance of the interaction between the spray and the surrounding air as an ignition controlling factor.

[Figure 11 about here.]

[Figure 12 about here.]

Additional evidence of the swirl motion influence on pilot flame progress is presented in Figure 13. It shows an image sequence of the ignition and flame progression of a pilot injection test at low rail pressure. Each image in this figure is a 20 repetitions ensemble average image, which have been calculated in order to have a representative picture of how pilot flame progresses. The sequence shows that the first luminosity spot is detected on the glow plug surface; later, this flame starts propagating toward the piston wall but also following the swirl motion within the combustion chamber. This sequence further evidences that within this time period (2500 to 6000μs) fuel speed is not much higher than the air speed (as shown in Figure 11) and for that reason swirl can influence fuel movement before ignition and the later flame progression.

[Figure 13 about here.]

4. Influence of glow plug temperature

4.1. Glow plug surface temperature measurement

The glow plug surface temperature has been measured by using a simplified version of the dual-wavelength thermometry method [30]. It is based on the Planck's law for black bodies and it has been extensively used for gray bodies by accounting with the surface emissivity [31, 32]. According to the method, the signal from an photo sensor viewing a radiating surface may be expressed as:

$$R_\lambda = \varepsilon_\lambda \cdot \frac{1}{\lambda^5} \cdot \frac{c_1}{e^{\frac{c_2}{T \cdot \lambda}} - 1} \tag{2}$$

where R_λ and ε_λ are the radiation intensity measured by the detector and the surface emissivity at a given wavelength (λ), respectively. T is the surface temperature and c_1 and c_2 are constants with values of $1.1910439E-16\ Wm^2/sr$ and $1.4388E-2\ mK$, respectively. T was calculated by measuring R at two different wavelengths and by assuming freely the ratio between both emissivities. Then, ε for each wavelength was recalculated introducing in Equation 2 the calculated temperature T and the corresponding value of R. This methodology is illustrated in Figure 14, in which T, ε_{694} and ε_{730} are plotted as a function of the emissivity ratio for a supply tension of 11 V. As can be observed, a wide range of possible temperature values as a function of the emissivity ratio was obtained for a given supply tension. This wide temperature range is later narrowed by accounting with the surface material emissivity found in the literature (0.4 to 0.9), as discussed later.

[Figure 14 about here.]

The material employed to build the whole glow plug tube, including the tip, is a $NiCr_{23}Fe$ alloy [33]. Specific information of its emissivity as a function of wavelength and temperature was not found, but related information has allowed to choose a range of possibilities. According to the material manufacturer [34], for a very similar nickel alloy ($NiCr_{15}Fe$) the total hemispherical emissivity ranges between 0.76 and 0.82 for temperatures from 923 K to 1253 K, respectively. And according to [35], the emissivity of these kind of alloys ranges between 0.42 and 0.58 for temperatures from 922 K to 1033 K. These emissivity values can not being taken as exact values but they can help to select the range of possibilities. For the temperatures measurements

shown in this paper the emissivity values will range from 0.4 to 0.9, which cover the range of possibilities found on the literature

Values of R at each wavelength were obtained after performing experimental measurements, calibration and image processing with the glow plug installed in an identical cylinder head out of the engine. The circuit current was controlled by means of a variable resistor and the supply tension was measured in the terminals of the glow plug, as in the engine tests. The radiation has been measured with an intensified camera installed in front of the glow plug at a few centimeters distance. The camera is a LaVision-Dynamight with a 16 bit CCD sensor at full resolution of 512 x 512. Two interference filters were used to isolate the radiation at each wavelength; a 694 and a 730 nm center wavelength filters with 10 nm bandwidth. The calibration was performed with a tungsten-ribbon lamp and the procedure is explained by Payri *et al* [36]. The digital levels were observed to be very uniform and an average value can be considered representative. Finally, these average digital levels at each wavelength and supply tension were converted into radiating intensity by means of the calibration function.

Figure 15 shows the possible range of temperatures on the glow plug tip as a function of the supply tension. The plot shows that temperature in the surface is approximately linear with supply tension. In addition, the plot shows that the uncertainty range of temperature calculated for a given voltage is of only around 35 K. These results actually help to enclose the range of possibilities within the glow plug works, which are very similar to the nominal values expected for a metallic glow plug [13].

[Figure 15 about here.]

4.2. Engine results

Engine results showing the influence of the glow plug temperature on pilot ignition are shown in Figure 16, in which LD and IL are plotted as a function of glow plug supply tension for a constant injection condition. For these tests, pilot probability is around 100% for all of them. Figure 16 shows a clear LD reduction if the supply tension is increased. Nevertheless, it must be observed that LD is reduced until a limit, approximately 1500 μs, from which not further reduction is observed (between 9.2 and 10.0 V). On the other hand, IL also shows a clear increase if supply tension is increased but it could be a consequence of the LD reduction. If ignition occurs earlier a larger amount of fuel is found around the glow plug. These results can be obvious in some way, since it is not strange that a temperature increase on the glow plug surface enhances ignition conditions. But, it is remarkable the fact that a temperature increase improves combustion only until certain value.

[Figure 16 about here.]

The glow plug temperature has a strong influence on ignition delay but above certain value its contribution is negligible. This experimental trend can be better understood by looking at the influence of temperature and fuel to air ratio on the predicted ignition delay calculated by means of CHEMKIN, which is shown in Figure 17. In this figure, a rectangle encloses the range of reachable temperatures, measured by means of 2-color method, and the range of possible fuel to air ratio, calculated by means of CFD. Within this range, an increase in temperature drastically reduces ignition delay, it can go from one millisecond to a few microseconds. It correlates very well with experimental

results. In addition, it is shown that at temperatures near 1200 K chemical ignition delays have been reduced as much as possible and a further increase in temperature do not necessarily represent a delay reduction. This fact leads to the conclusion that any improvement on cold start pilot ignition must be done by controlling the fuel transport processes after injection since current glow plug technology already reaches such temperatures.

[Figure 17 about here.]

5. Summary and conclusions

A detailed study on the influence of the spray-glow plug configuration on ignition and combustion progress under cold start conditions has been presented. Experimental tests have been carried out in a specially adapted facility which allows to reproduce, systematically, low speed and low temperature conditions as those reached by a passenger car diesel engine at $-20°C$ during start. In this facility, in-cylinder pressure analysis can be coupled with high speed visualization which has allowed to characterize pilot flame ignition and progress. Specific CFD calculations were carried to assist understanding of the phenomena that control this combustion process.

Spray-glow plug configuration has shown to have a clear influence on ignition of the pilot flame, which at the same time promotes a proper start of combustion a few hundreds of microseconds after the start of the main injection. This early start of combustion allows that combustion progresses controlled by the momentum induced by the spray during injection burning a larger amount of fuel.

Ignition of the pilot injection is controlled by the glow plug temperature and the fuel to air ratio on its vicinity. The temperature of the glow plug surface reduces ignition delay by accelerating the chemical kinetics that lead to ignition. However, above a given temperature value this reduction starts to be negligible. For this reason, the most limiting factor on pilot ignition is not the glow plug temperature but the fuel to air ratio on the glow plug vicinity. In this regard, fuel to air ratio is not directly controlled by the injection process but by the air motion existing after end of injection, which are originated by the injection event and by swirl.

References

[1] Yassine, M.K., Tagomori, M.K., Henein, N.A., Bryzik, W.. White smoke emissions under cold starting of diesel engines. SAE Paper 960249 1996;.

[2] Peng, H., Cui, Y., Shi, L., Deng, K.. Effects of exhaust gas recirculation (egr) on combustion and emissions during cold start of direct injection (di) diesel engine. Energy 2008;33(3):471 – 479. doi: 10.1016/j.energy.2007.10.014.

[3] Peng, H.Y., Cui, Y., Deng, H.Y., Shi, L., Li, L.G.. Combustion and emissions of a direct-injection diesel engine during cold start under different exhaust valve closing timing conditions. Proceedings of the Institution of Mechanical Engineers, Part D: Journal of Automobile Engineering 2008;222(1):119–129.

[4] Weilenmann, M., Favez, J., Alvarez, R.. Cold-start emissions of

modern passenger cars at different low ambient temperatures and their evolution over vehicle legislation categories. Atmospheric Environment 2009;43(15):2419–2429.

[5] Broatch, A., Ruiz, S., Margot, X., Gil, A.. Methodology to estimate the threshold in-cylinder temperature for self-ignition of fuel during cold start of diesel engines. Energy 2010;35:2251–2260.

[6] Pacaud, P., Perrin, H., Laget, O.. Cold start on diesel engine: Is low compression ratio compatible with cold start requirements? SAE Paper 2008-01-1310 2008;.

[7] Laget, O., Pacaud, P., Perrin, H.. Cold start on low compression ratio diesel engine: Experimental and 3D RANS computation investigations. Oil and Gas Science and Technology Rev IFP 2009;64(3):407–429.

[8] MacMillan, D., La Rocca, A., Shayler, P.J., Murphy, M., Pegg, I.G.. The effect of reducing compression ratio on the work output and heat release characteristics of a DI diesel under cold start conditions. SAE Paper 2008-01-1306 2008;.

[9] Johnson, T.V.. Review of CO_2 emissions and technologies in the road transportation sector. SAE paper 2010;2010-01-1276. doi:10.4271/2010-01-1276. URL `http://papers.sae.org/2010-01-1276`.

[10] Johnson, T.V.. Review of diesel emissions and control. SAE paper 2010;2010-01-0301. doi:10.4271/2010-01-0301. URL `http://papers.sae.org/2010-01-0301`.

[11] Payri, F., Broatch, A., Serrano, J.R., Rodríguez, L.F., Esmorís, A.. Study of the potential of intake air heating in automotive DI diesel engines. SAE Paper 2006-01-1233 2006;.

[12] Kowalewicz, A.. Combustion systems of high-speed piston internal combustion engines. New York: Elsevier science publishers; 1984.

[13] Lindl, B., Schmitz, H.. Cold-start equipment for diesel direct-injection engines. SAE Paper 1999-01-1244 1999;.

[14] Kern, C., Dressler, W., Lindemann, G., Rothacker, V.. An innovative glow system for modern diesel engines. SAE paper 1999-01-1240 1999;.

[15] Walter, B., Perrin, H., Dumas, J.P., Laget, O.. Cold operation with optical and numerical investigations on low compression ratio diesel engine. SAE Paper 2009-01-2714 2009;.

[16] Pastor, J.V., García-Oliver, J.M., Pastor, J.M., Ramírez-Hernández, J.G.. Experimental facility and methodology for systematic studies of cold startability in direct injection diesel engines. Meas Sci Technol 2009;20(095109). doi:10.1088/0957-0233/20/9/095109.

[17] Pastor, J.V., García-Oliver, J.M., Pastor, J.M., Ramírez-Hernández, J.G.. Ignition and combustion development for high speed direct injection diesel engines under low temperature cold start conditions. Fuel 2011;90(4):1556 – 1566.

[18] Payri, F., Molina, S., Martín, J., Armas, O.. Influence of measurement errors and estimated parameters on combustion diagnosis. Applied Thermal Engineering 2006;(26):226 – 236.

[19] Torregrosa, A., Olmeda, P., Degraeuwe, B., Reyes, M.. A concise wall temperature model for di diesel engines. Applied Thermal Engineering 2006;(26):1320 – 1327.

[20] Soid, S., Zainal, Z.. Spray and combustion characterization for internal combustion engines using optical measuring techniques - a review. Energy 2011;36(2):724 – 741. doi:10.1016/j.energy.2010.11.022.

[21] Merola, S.S., Sementa, P., Tornatore, C., Vaglieco, B.M.. Effect of the fuel injection strategy on the combustion process in a pfi boosted spark-ignition engine. Energy 2010;35(2):1094 – 1100. doi:10.1016/j.energy.2009.06.002. ECOS 2008, 21st International Conference, on Efficiency, Cost, Optimization, Simulation and Environmental Impact of Energy Systems.

[22] Kee, R., Rupley, F., Miller, J.. Chemkin II: A fortran chemical kinetics package for the analysis of a gas-phase chemical kinetics. Tech. Rep.; Sandia Laboratories; 1993.

[23] Curran, H.J., Gaffuri, P., Pitz, W.J., Westbrook, C.K.. A comprehensive modeling study of n-Heptane oxidation. Combustion and Flame 1998;114:149–177.

[24] Star-CD Methodology, Version 3.26. CD-Adapco; 2005.

[25] Dukowicz, J.K.. A particle-fluid numerical model for liquid sprays. Journal of Computational Physics 1980;35(2):229–253.

[26] Huh, K.Y., Gosman, A.. A phenomenological model of diesel spray

atomization. In: Proceedings of the International Conference on Multiphase Flows. 1991,.

[27] Reitz, R.D., Diwakar, R.. Structure of high-pressure fuel sprays. SAE Paper 870598 1987;.

[28] Habchi, C., Lafossas, F.A., Beard, P., Broseta, D.. Formulation of a one-component fuel lumping model to assess the effects of fuel thermodynamic properties on internal combustion engine mixture preparation and combustion. SAE Paper 2004-01-1996 2004;.

[29] Chartier, C., Aronsson, U., Andersson, Ö., Egnell, R.. Effect of injection strategy on cold start performance in an optical light-duty DI diesel engine. SAE Paper 2009-24-0045 2009;.

[30] Meriaudeau, F.. Real time multispectral high temperature measurement: Application to control in the industry. Image and Vision Computing 2007;25:1124–1133.

[31] Maswadeh, W., Tripathi, A., Arnold, N.S., DuBow, J., Meuzelaar, H.L.. High speed, two-wavelength radiation thermometry of single micro particles during co2 laser heating. Journal of Analytical and Applied Pyrolysis 1994;28(1):55 – 70. doi:DOI: 10.1016/0165-2370(93)00756-D.

[32] Tago, Y., Akimoto, F., Kitagawa, K., Arai, N.. Measurements of surface temperature and emissivity by two-dimensional four-color thermometry with narrow bandwidth. Energy 2005;30(2-4):485 – 495. doi: 10.1016/j.energy.2004.09.007.

[33] Eller, M.D.. Patent: Protection tubes for sensors or glow elements. Tech. Rep. EP0945724; 1999. URL http://www.freepatentsonline.com/EP0945724A2.html.

[34] http://www.specialmetals.com/products/inconelalloy600.php; ????

[35] Wilson, J.S.. Sensor technology handbook. Elsevier Inc.; 2005. ISBN 978-0-7506-7729-5.

[36] Payri, F., Pastor, J.V., García, J.M., Pastor, J.M.. Contribution to the aplication of two-colour imaging to diesel combustion. Measurement Science and Technology 2007;18:2579–2598. doi:10.1088/0957-0233/18/8/034.

List of Figures

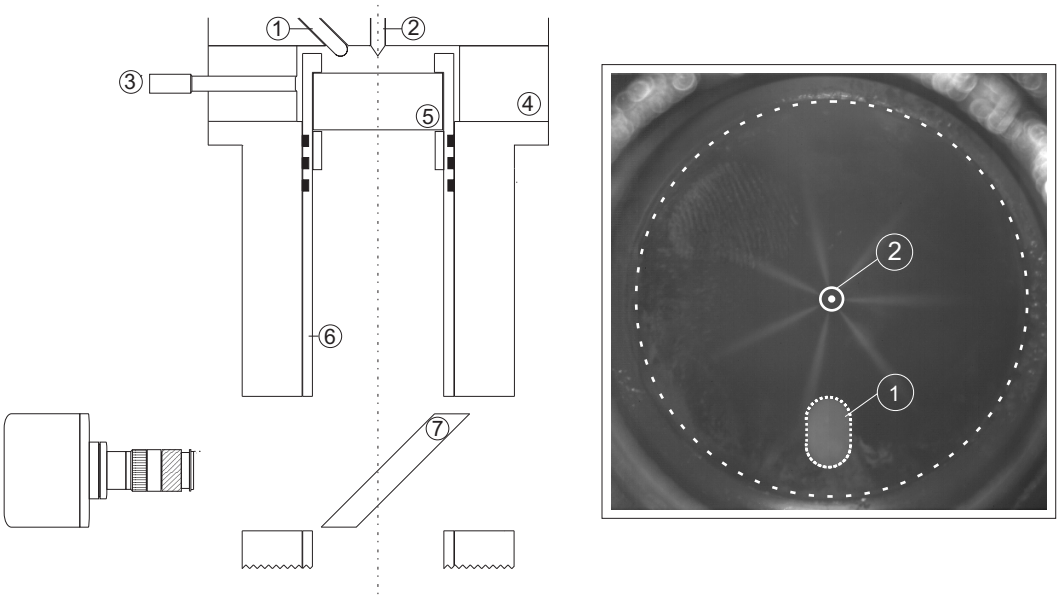

Figure 1: Sketch of the optical access in the single cylinder engine and an image showing how the combustion chamber is seen from the camera point of view. 1.- Glow plug, 2.- Injector nozzle, 3.- Pressure transducer, 4.- Aluminum piece, 5.- Sapphire window, 6.- Elongated piston, 7.- Elliptical UV mirror.

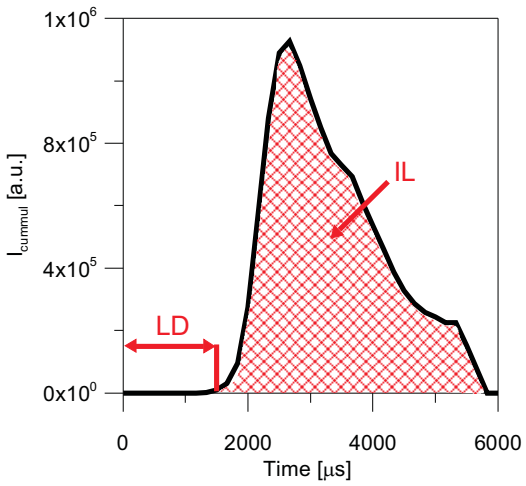

Figure 2: I_{cumul} as a function of time for a pilot injection test. The LD is defined as the time from SoI to flame appearance. And, IL is defined as the area under the I_{cumul} trace.

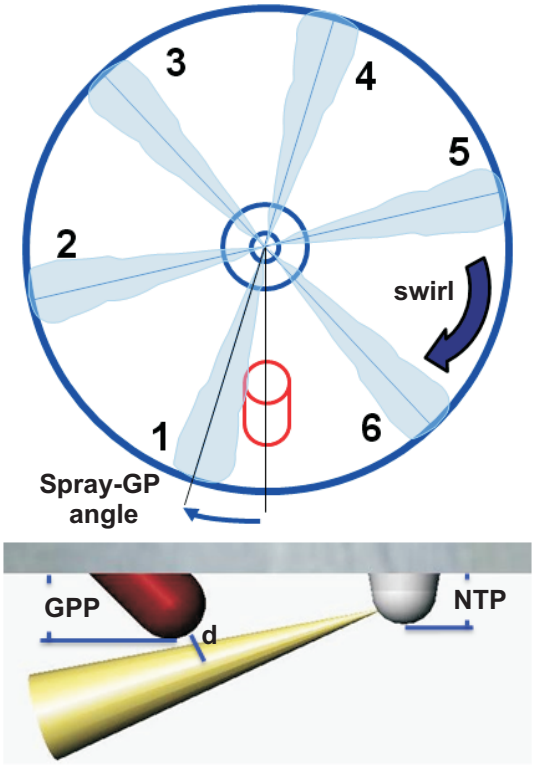

Figure 3: Sketch of the relative position between the glow plug and one of the sprays. In the top, the figure shows the direction of the swirl and how the orientation angle is measured. In the bottom, the variation of the NTP and GPP are shown.

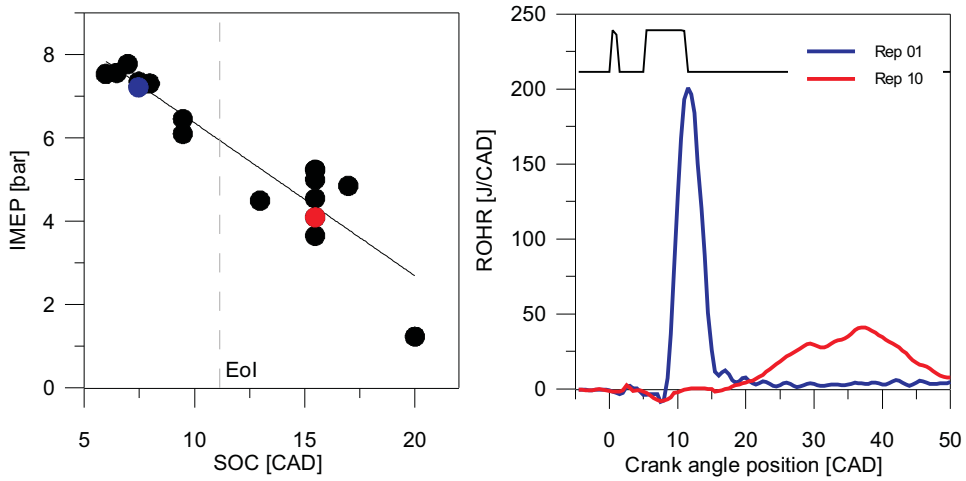

Figure 4: On the left side, IMEP vs. SOC for the 30 repetitions of a full injection strategy test with an orientation angle of -10 *grad* at the high level of injection pressure. The EoI is marked as a reference of the injection duration. On the right side, ROHR versus crank angle position for two of the cycles shown on the right side. The full injection strategy consists on a pilot injection pulse of 6 mg which starts at 0 CAD followed, at 5 CAD, by the main injection pulse of 24 mg

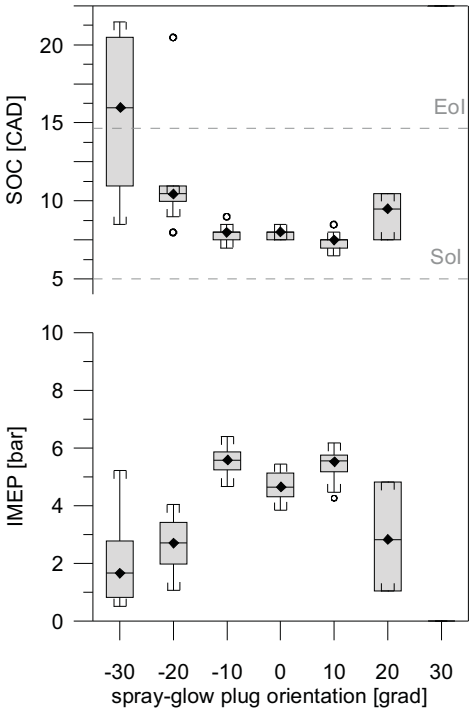

Figure 5: SOC (top) and IMEP (bottom) as a function of the spray-glow plug orientation angle for full injection tests at the low level of rail pressure. The outliers (unfilled dots) are points out of the range defined by 1.5 times the interquartile range.

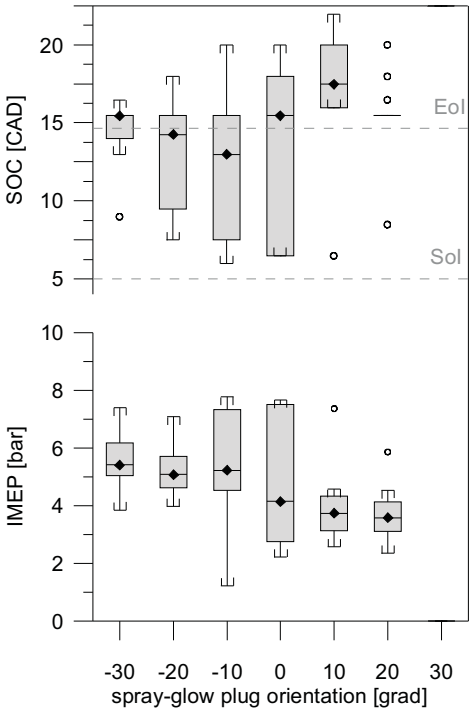

Figure 6: SOC (top) and IMEP (bottom) as a function of the spray-glow plug orientation angle for full injection tests at the high level of rail pressure. The outliers (unfilled dots) are points out of the range defined by 1.5 times the interquartile range.

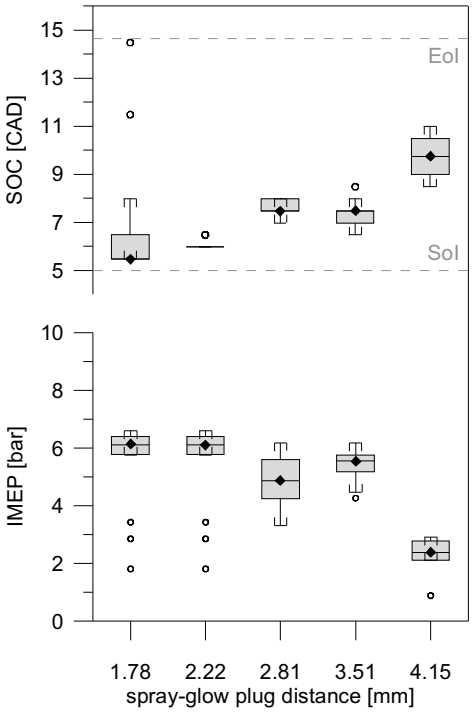

Figure 7: SOC (top) and IMEP (bottom) as a function of the spray-glow plug distance for full injection tests at the low level of rail pressure. The outliers (unfilled dots) are points out of the range defined by 1.5 times the interquartile range.

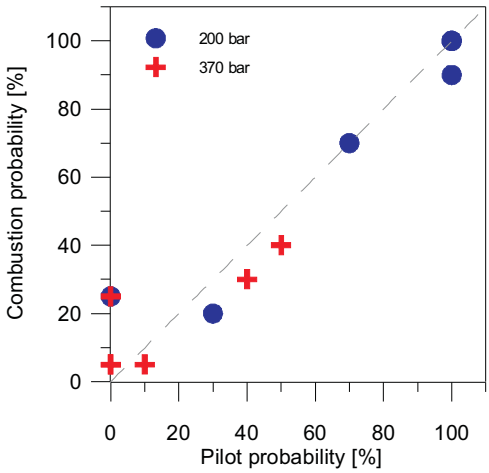

Figure 8: Combustion probability, calculated for the full injection strategy, of early burning cycles ($IMEP > 0$ and $SOC < EOI$) as a function of pilot probability, measured for the pilot single injection in independent tests. The tests presented in this figure corresponds to the six orientation configurations tested at both levels of injection pressure

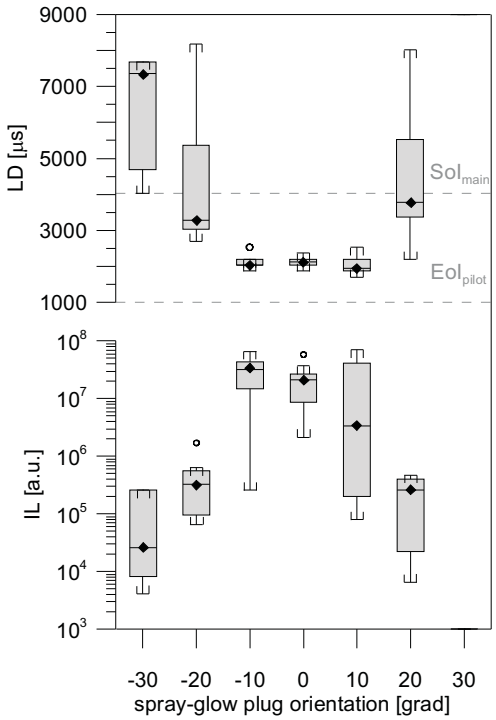

Figure 9: LD (top) and IL (bottom) as a function spray-glow plug orientation angle for the cases at low rail pressure. In the LD plot the EoI_{pilot} and SoI_{main} are marked with a dashed line as a reference to the injection event. The outliers (unfilled dots) are points out of the range defined by 1.5 times the interquartile range

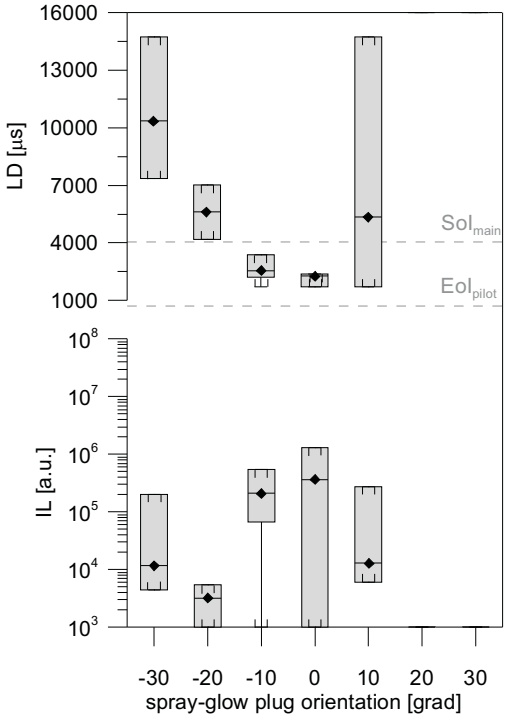

Figure 10: LD (top) and IL (bottom) as a function spray-glow plug orientation angle for the cases at high rail pressure. In the LD plot the EoI_{pilot} and SoI_{main} are marked with a dashed line as a reference to the injection event. The outliers (unfilled dots) are points out of the range defined by 1.5 times the interquartile range

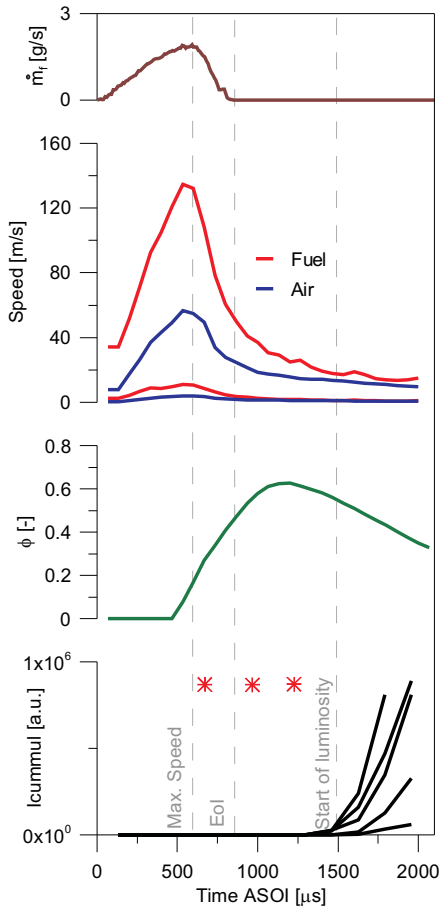

Figure 11: Experimental and CFD results versus time after start of injection for a 6 mg single injection case at low level of injection pressure. First on the top, mass flow rate per orifice (measured). Second from top to bottom, fuel and air maximum and minimum speeds in a plane that contains both axes, the cylinder axis and the axis of the spray that is closest to the glow plug. Third from top to bottom, fuel to air ratio on the glow plug close vicinity. And in the bottom, I_{cummul} for five repetitions of a visualization test under the same conditions. Marked with gray lines are the moment at which fuel reaches its maximum speed, the EoI and the moment at which the camera detects the first luminosity spots

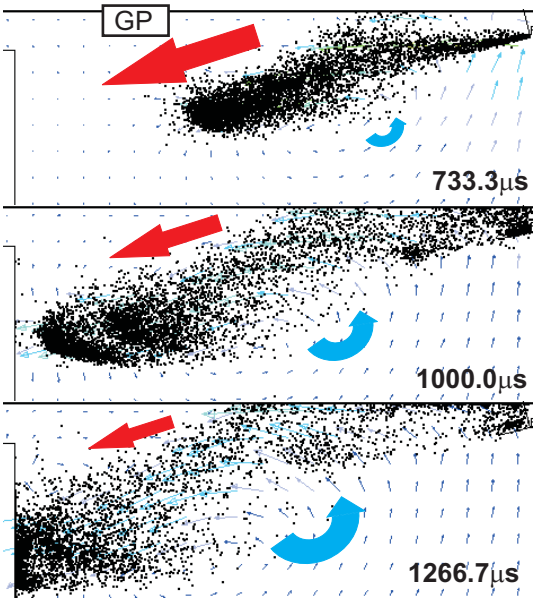

Figure 12: Fuel drops and air velocity vectors in a plane that contains the cylinder axis and the closest to the glow plug spray axis. Three different time instants have been selected, they are marked with asterisks on Figure 11 and written on the right-bottom side of each figure.

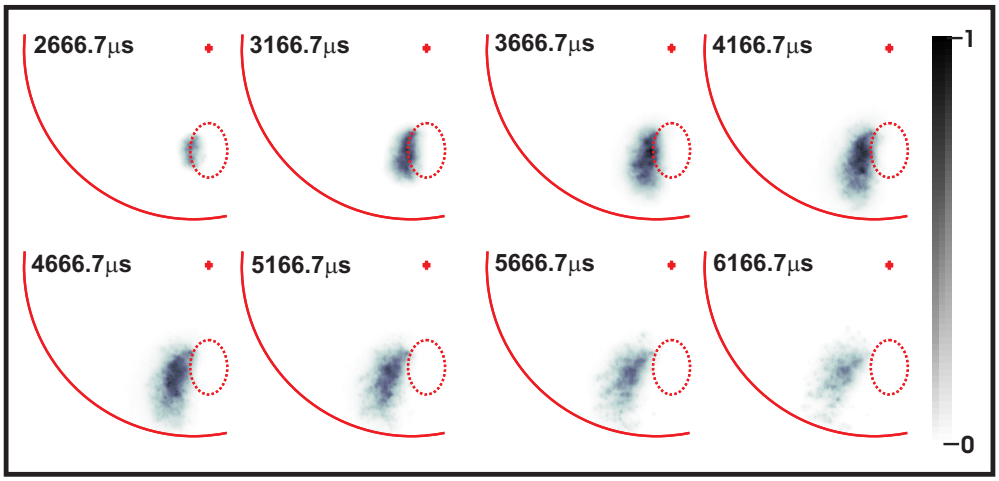

Figure 13: Sequence of images showing pilot ignition and flame progression for a low rail pressure case with an orientation of $-10°$. Each image shown is an average image of 20 repetitions (all with luminosity) acquired in a pilot injection test. The acquisition time after start of injection is shown in the top left corner of each picture. The window border, glow plug and nozzle position are sketched in red color. The average digital levels have been normalized with respect to the sequence maximum and the color scale is shown on the right side

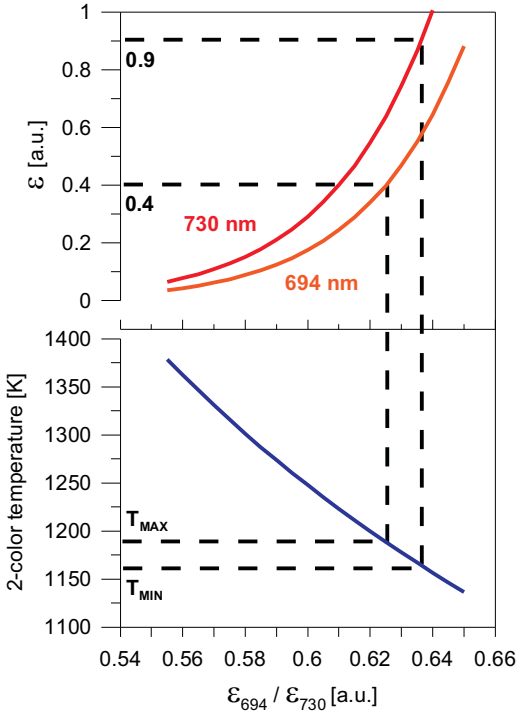

Figure 14: 2-color temperature and surface emissivity for two wavelengths, 730 and 694 nm, as a function of the emissivity ratio. This example shows the methodology used to estimate the possible range of temperatures that the glow plug tip has for a supply tension 11 V.

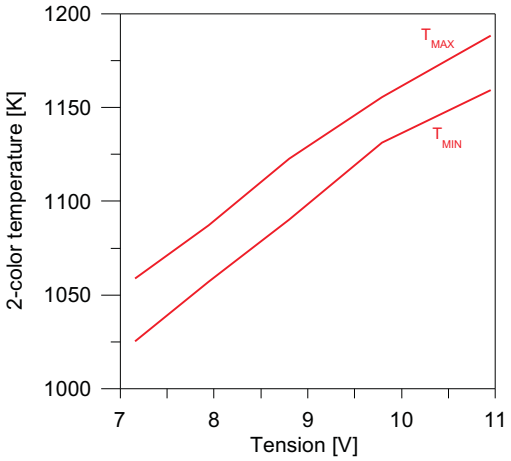

Figure 15: 2-color temperature range as a function of the supply tension.

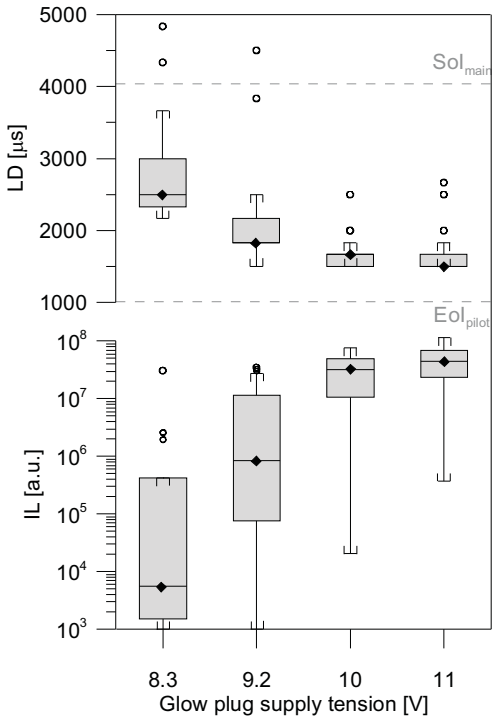

Figure 16: LD (top) and IL (bottom) as a function of the supply glow plug tension at the low level of rail pressure. In the LD plot the EOI is marked with a dashed line as a reference to the injection event. The outliers (unfilled dots) are points out of the range defined by 1.5 times the interquartile range. The injection condition is a single injection of 6 mg injected at 0 CAD.

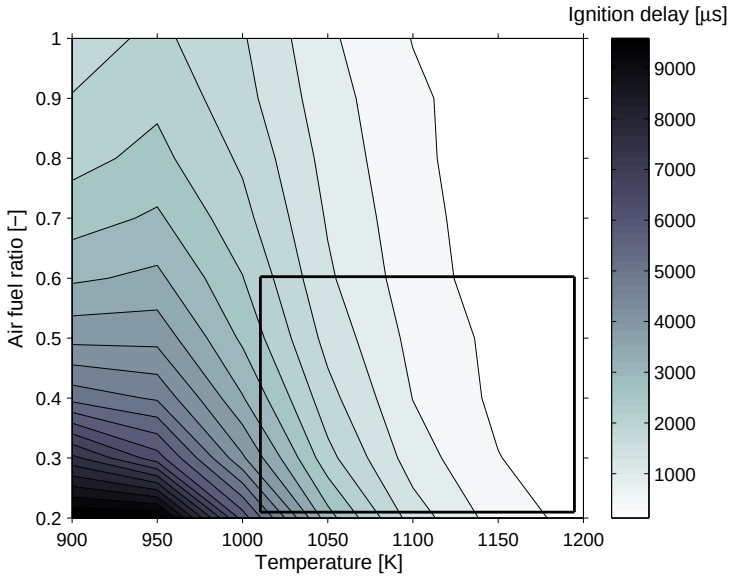

Figure 17: n-Heptane predicted ignition delay as a function of equivalence ratio and temperature at a constant pressure of 27 *bar*.

List of Tables

Table 1: Abbreviations

Nomenclature			
I	light intensity, -	EoI	end of injection
$\dot{m}$	mass flow, g/s	EVO	exhaust valve opening
R	radiance, $W/(sr \cdot m^2 \cdot nm)$	GP	glow plug
T	temperature, K	GPP	glow plug protrusion
Subscripts		HRL	heat release law
cummul	accumulated	IDI	indirect diesel injection
f	fuel	IL	integrated luminosity
main	main injection	IMEP	indicated mean effective pressure
pilot	pilot injection	IVC	intake valve closing
Greek symbols		LD	luminosity delay
α	crank angle degree	LHV	lower heating value
λ	wavelength	NTP	nozzle tip protrusion
Abbreviations		ROHR	rate of heat release
CAD	crank angle degree	SOC	start of combustion
CCD	charge-coupled device	SoI	start of injection
CFD	computational fluid dynamics	UV	ultraviolet
CMOS	compl. metal oxide semiconductor		
CR	compression ratio		
ECU	engine control unit		

Table 2: Parametric variation

Parameter	Variation
Spray-glow plug orientation [°]	-30, -20, -10, 0, 10 and 20
Glow plug protrusion (GPP) [mm]	3, 4.4 and 5.8
Nozzle tip protrusion (NTP) [mm]	1.1, 2.1 and 2.9
Supply tension [V]	7, 8.3, 9.2 and 10

Table 3: Spray-glow plug distance (units in mm)

NTP	GPP	d
1.1	3	2.81
2.1	3	3.51
2.9	3	4.15
2.1	4.4	2.22
2.1	5.8	1.78